Research Article

BIOMEDICAL Journal of Scientific & Technical Research

ISSN: 2574 -1241

DOI: 10.26717/BJSTR.2022.41.006604

# Synthesis of CVD Diamond Nanoparticles and Cytotoxicity Evaluation in Murine Metastatic Melanoma Cells

**Cristiane Da Costa Wachesk[1,4]*, Carolina Ramos Hurtado[1,2], Rebeca Falcão Borja De Oliveira Correia[1,4], Dayane Batista Tada[1], Getúlio Vasconcelos[3], Evaldo José Corat[4] and Vladimir Jesus Trava Airoldi[4]**

[1]*Laboratory of Nanomaterials and Nanotoxicology, Institute of Science and Technology, Federal University of São Paulo (UNIFESP), Brazil*

[2]*Federal Institute of São Paulo (IFSP), Brazil*

[3]*Laboratory of Lasers and Optical Applications Development, Dedalo, Institute of Advanced Studies (IEAv), Coronel Aviador José Alberto Albano do Amarante, Brazil*

[4]*Associated Laboratory of Sensors and Materials, National Institute for Space Research (INPE), Brazil*

***Corresponding author:** Cristiane da Costa Wachesk, Laboratory of Nanomaterials and Nanotoxicology, Institute of Science and Technology, Federal University of São Paulo (UNIFESP), Associated Laboratory of Sensors and Materials, National Institute for Space Research (INPE), Brazil

**ARTICLE INFO**

**Received:** January 18, 2022

**Published:** January 28, 2022

**Citation:** Cristiane Da Costa Wachesk, Carolina Ramos Hurtado, Rebeca Falcão Borja De Oliveira Correia, Dayane Batista Tada, Getúlio Vasconcelos, et al., Synthesis of CVD Diamond Nanoparticles and Cytotoxicity Evaluation in Murine Metastatic Melanoma Cells. Biomed J Sci & Tech Res 41(3)-2022. BJSTR. MS.ID.006604.

**Keywords:** HFCVD Diamond; Laser Ablation; CVD Diamond Nanoparticles (CVD-DNPs); Drug Delivery; Melanoma

**ABSTRACT**

Diamond nanoparticles (DNPs) have demonstrated *in vitro* and *in vivo* biomedical applicability due to their low toxicity and biocompatibility. Recent studies have focused on the potential use of DNPs as suitable vehicles to improve drug delivery in cancer treatment. The advantages of DNPs lie in their high stability and small size compared to other carbon-based nanomaterials. In this work, CVD-diamond nanoparticles (CVD-DNPs) were synthesized and evaluated for their application as a new drug delivery platform for metastatic melanoma therapy. A new synthesis technique developed DNPs from CVD diamond thin film. This type of diamond has the same physical and chemical properties as a natural diamond: extreme hardness, excellent thermal conductivity, low coefficient of friction, biocompatibility, and is chemically inert at temperatures below 800 °C. The main objective of this study was to produce CVD-DNPs by laser ablation and evaluate their cytotoxicity. A pulsed, ytterbium-doped fiber (Yb) was used to form DNPs in pure aqueous medium (Milli-Q). The final suspension was obtained at high concentration of the CVD-DNPs and was used to evaluate the cytotoxicity in murine metastatic melanoma B16-F10 cells by using colorimetric assays. The characterization by FT-IR, X-Ray, DLS, RAMAN, SEM, and TEM demonstrated the successful synthesis of CVD-DNPs with a hydrodynamic diameter of 57 and 54 nm. *In vitro* studies performed for 24 h and 48 h resulted in 70–80% viability of cells incubated with CVD-DNPs at 250 µg/mL, which demonstrated an insignificant cytotoxic effect. Thus, these results suggest the potential use of CVD-DNPs as a drug delivery platform for antitumoral therapy.

**Abbreviations:** DNPs: Diamond Nanoparticles; EPR: Enhanced Permeability and Retention; HFCVD: Transmission Hot-Filament Chemical Vapor Deposition; DLS: Dynamic Light Scattering; TEM: Dynamic Light SEM-FEG: Scattering Electron Microscopy Field Emission Scanning Electron Microscopy; ANOVA: One-Way Analysis of Variance; SEM: Scanning Electron Microscopy; PS: Photosensitizers

## Introduction

Diamond has a diversity of extraordinary properties that continue to attract scientific interest in the search for new technological applications [1-3]. This widespread interest has led to new approaches to grow and process diamonds and diamond films [4]. A series of applications have been developed based on the combination of diamond properties and the multiplicity of film properties obtained by combining the microstructure, morphological surface, impurities, and surfaces [4,5]. Diamond Nanoparticles (DNPs) are a class of carbon-based nanomaterials of increasing interest in science and technology [3], including their use as a drug delivery [4]. DNPs are inert [5], optically transparent, photoluminescent [6], and biocompatible [7]. The application of DNPs as a drug delivery platform for cancer therapy is based on the known passive tumor targeting due to the enhanced permeability and retention (EPR) effect of NPs with 30–100 nm. The efficiency of DNPs as drug delivery has been proven to be a result of increased vascular permeability provided by DNPs [4,8]. Additionally, DNPs have been shown to remain inside the cell for a longer period of time, increasing the efficiency of chemotherapeutic treatment. These effects are probably a result of the cell internalization of DNPs by endocytosis [8], which may eventually carry also external compounds into the cell due to their complexation with DNPs [9]. Since DNPs can bind tightly to a variety of molecules and deliver them directly to a tumor [10], the use of DNPs as delivery agents considerably reduces the toxic side effects of chemotherapy [11]. Therefore, DNPs are a useful tool in the search for better drug administration against cancer via an induced permeability of vascular barrier [3,12].

As with all commercial applications, cost-efficient production methods are as important as the application itself. Current research has focused on how DNPs can be synthesized through explosions. More recent studies indicate that the synthesis of detonation DNPs has already been optimized for a commercial scale, with rigid structure clusters that can reach hundreds of nanometers or even several micrometers [12]. Therefore, for most of its applications, particularly in biology and medicine, DNPs must be purified after synthesis [13]. Other ways to synthesize may be classified in two approaches: "bottom-up", when atoms are aggregated to originate the nanomaterial, and "top-down", when the material is removed from a bulk structure [14,15]. Pulsed laser ablation used in. this study is a top-down approach and is gaining special attention within the scientific community [16-18]. This study focused on producing low-cost CVD-Diamond Nanoparticles (CVD-DNPs) and their cytotoxicity, to evaluate a possible application as drug delivery platform. To synthesize CVD-DNPs, the Synthetic CVD-diamond was obtained by an innovative technology manufacturing from the CVDVale company. The CVDVale uses hot-filament chemical vapor deposition (HFCVD), which makes the CVD diamonds suitable for implantable medical, dental, and drug delivery interests. This work addresses the use of LASER ablation and evaluates the impact of this technique on the particle size, morphology, and cytotoxicity of CVD-DNPs.

## Materials and Methods

### CVD Diamond Productions

For diamond film growth, the HFCVD reactor employed composed of a set of 6 tungsten filaments, with 125-μm diameter and 4-mm equidistant, maintained at a temperature of approximately 2200°C. The total gas pressure was 50 Torr during the 3 h of growth. The reactive gas mixture consisted of 2% CH4 and 98% H2. The ramp downturn off period was 1h. The sample was placed on the substrate holder at a distance of 5 mm for growth at 700°C, which was approximately 0.43 μm/h and 10 mm for growth at 550°C. An approximately 30 to 50 micrometer microcrystalline diamond was grown in columnar structure without re-nucleation. This is process was used at CVDVale, which is a company specialized in the CVD-diamond coating.

### Synthesis and Preparation of the CVD Nano-Diamond Suspensions

To perform the laser ablation process, we used CVD-diamond film obtained via the HFCVD technique provided from the CVDVale Company. CVD diamond film, 30 μm thick, was macerated using an agate mortar and pestle, and sifted in a granulometry sieve of 200 mesh (0.074 mm of mesh opening). CVD-diamond 5 mg/mL aqueous suspensions from Deionizer Millipore Milli-Q system (40 mL volume) were prepared and irradiated by pulsed laser ablation of ytterbium-doped fiber (Yb) (λ=1062nm) using the PRO Marking (Pulsed Fiber-Yb laser), as shown in (Figure 1). The CVD-DNPs were ablated for 30 (i) and 60 (ii) min. Next, the colloidal suspension was centrifuged in a Hettich Rotina 4500 RPM for 0 and 60 min, respectively, to remove aggregates, shown in (Table 1). Hydrofluoric acid(HF) was used to remove SiO2 contamination from the sample due to abrasion in the Agate mortar. To reduce the size of CVD-NDs, at 30 (i) and 60 (ii) min, the colloidal suspensions were centrifuged for 0 and 60 min, respectively, as shown in (Table 1). The CVD-DNPs were obtained by the laser ablation method. Using a gaussian laser beam, pulsed average power 20 W, pulse time of 200 ns, and frequency of 45 (KHz), the irradiance is obtained by:

$$I\left(w/cm^2\right)=\frac{2.P_{k(w)}}{\pi.r^2}\ ;\ (1)$$

Where,

$$P_k=\frac{P_M}{f(H_z).t_p(s)}\ (2)$$

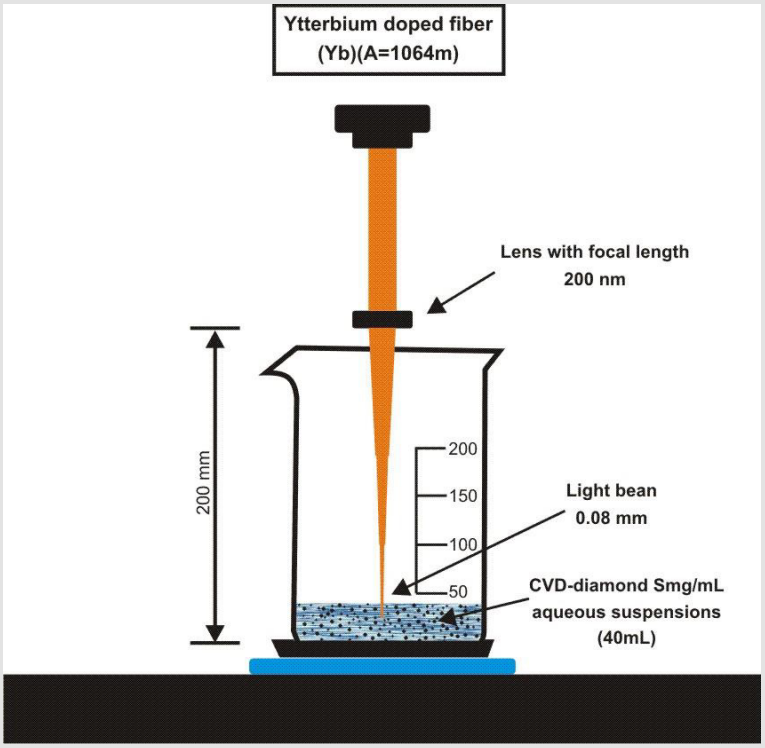


**Figure 1:** Draft pulsed laser ablation of ytterbium doped fiber (Yb) (λ=1064nm) PRO Marking (Pulsed Fiber-Yb laser).

**Table 1:** CVD-DNPs synthesis by pulsed laser ablation of ytterbium doped fiber (Yb) (λ=1064 nm).

| Samples | Time laser ablation (min) | Current Pen | Loop Count | Speed (MM/Scans) | Power % | Frequency (KHz) | Pulse Time) | Start TC (US) | Laser Off TC (US) | End TC (US) | Polygon TC (US) |
|---|---|---|---|---|---|---|---|---|---|---|---|
| CVD-DNPs (i) | 30 | 0 | 1 | 500 | 100 | 45 | 200 | 300 | 100 | 300 | 100 |
| CVD-DNPs (ii) | 60 | 0 | 1 | 500 | 100 | 45 | 200 | 100 | 100 | 300 | 100 |

and where the minimum beam Ø is 0.04 mm, obtained by:

$$W_{\min} = \frac{\lambda . f}{\pi . w_o} \text{ ; (3)}$$

Where,

$\lambda$=1064 $nm$ ($(beam\ length)$), $f$=190 $nm$ ($focal\ distance$),and where $w0$=10 $mm$ ($beam\ diameter$ "in");

Which results in:

$$I\left(W/cm^2\right) \sim 10^9 \left(W/cm^2\right) \text{ (4).}$$

However, considering that this beam radiated particles of 10 micrometers of edge during the experiment, these microparticles when irradiated in the highest energy region of the beam (central region) were probably ablated.

## Characterization Techniques

**Dynamic Light Scattering (DLS) and Zeta Potential**: Hydrodynamic diameter, size distribution, and ζ-potential values were obtained through the dynamic light scattering (DLS) technique. The equipment used for this analysis was the DelsaTM Nano C by Beckman Coulter, belonging to ICT-UNIFESP multi-user NAPCEM laboratory. For each sample, the dilutions were made in deionized water and the measurements were performed in triplicate to obtain mean and standard deviation values, both generated by the equipment software.

## Raman Scattering Spectroscopy

The Raman scattering spectra were obtained using the Horiba Scientific equipment with a helium cadmium laser excitation (325 nm), from LAS/INPE. This vibrational spectroscopy technique is employed to determine molecular structures, quantification, materials identification, and the degree of crystalline network disorder information. Raman spectroscopy was also used to identify different forms of carbon.

**X-Ray Diffractometry:** The diffractograms were obtained using the PAN alytical brand system from the X'PertPro series, from LAS-INPE and operated at 45kV and 40 mA. This technique was

used to identify and quantify crystalline phases, orient crystallites, determine single cell parameters, and residual stress [19].

**FT-IR (Fourier Transformed Infrared Spectroscopy):** The infrared spectra were acquired by Fourier transform infrared spectroscopy using a universal attenuated total reflectance sensor (FT-IR-UATR) (Perkim Elmer Spectrum, model Frontier). The FT-IR spectrum was an average of 32 scans at a speed of 2 s per scan in a range of 400–4000 $cm^{-1}$. The resolution of the spectrometer was of 4 $cm^{-1}$.

**Field Emission Scanning Electron Microscopy (SEM-FEG):** CVD-DNPs were physically and morphologically characterized using a scanning electron microscope. The micrographs were performed in collaboration with the LAS/INPE group and obtained with Field Emission Scanning Electron Microscopy by Tescan Mira 3, MIRA 3 model, which was coupled to the X-Ray dispersive energy spectroscopy (EDS) system.

**Transmission Electron Microscopy (TEM):** The micrographs were obtained using the Transmission Electron Microscope MET Tecnai G2 Spirit Bio TWIN 120 kV (FEI) with a digitally controlled system, CompuStage Single-Tilt tilt support, Olympus-SIS Veleta CCD 120/200 kV digital camera, tungsten emitter (W), TIA (TEM Imaging and Analysis) program for image visualization, in collaboration with the Institute of Advanced Studies of the Sea (IEAMar), UNESP.

### *In vitro* Assays

**Cell Culture and Cell Line:** The B16F10-Nex2 cell line studied here as a tumor cell model was kindly provided by the Laboratory of experimental biology of cancer (LABEC-UMC, BR). Tumor line B16 was isolated from spontaneous melanoma in C57Bl/6 animals. Fidler [20] obtained gradually more aggressive and invasive strains after successive *in vivo* passages, numbering them from F1 to F10. The most aggressive strain was B16F10, obtained from the Ludwig Institute for Cancer Research. B16F10-Nex2 cells were maintained at 5% CO2 at 37°C and grown in medium RPMI-1640 (GIBCO) composed of vitamins, amino acids, salts, D-glucose, 24 mM sodium bicarbonate, 40 mg/mL gentamicin (GIBCO), and supplemented with 10% fetal bovine serum (SFB) (Cultilab), pH 7.4. For cell washing, the buffer was PBS (Phosphate Buffer Saline) with composition of 140 mM of NaCl, 2.7 mM, KCl, 10 mM of Na2HPO4, and 1.8 mM of KH2PO4, pH 7.4). Since B16F10-Nex2 cells are adherent, trypsin (GIBCO) was used to release cells from culture flasks and plates.

**Analysis of Cell Viability:** The cell viability assay was based on the indirect measurement of mitochondrial activity of cells after incubation with the materials under study. In viable cells, the salt 3-[(4,5-dimethylthiazol-2-yl)-2,5-diphenyltetrazolium bromide] (MTT) (Sigma-Aldrich) was reduced and forms formazan, which is a purple insoluble salt. The formazan was quantified by absorbance measurement after solubilization in organic solvent. In this study, B16 cells were cultivated in RPMI1640 culture medium and plated in 96-well plates at the concentration of 103 cells per well (300 µL). After 12 h, the supernatant was removed, and the cells were incubated with 50 µL of 5 different concentrations of CVD-DNPs suspension. After the incubation period of 24 and 48 h, the culture medium was removed and 100 µL of MTT solution (2 mg/mL, PBS solvent) was added in each well. The MTT was removed 3 h later, and the formazan salt was solubilized with 200 µL of DMSO. The solution was left to rest for 30 min,followed by measurement of absorbance at 540 nm in a plate reader (Biotek). Absorbance of the wells where the cells were incubated in the absence of NDs were considered as 100% of viability.

**Statistical Analysis:** The assays were performed in quintuplet, expressed as mean ± standard deviation and mean ± mean standard error of MTT assays. All the assays were statistically analyzed by Graphpad Prism® software, using the one-way analysis of variance (ANOVA), followed by the Bonferroni test to compare with the control group. A probability value equal or less than 0.05 was considered statistically significant.

## Results and Discussion

The relationship between the morphology of diamond crystals and the conditions of their crystallization has been the subject of great scientific debate in the last two centuries. Based on the analysis of external morphology and diamond surface, Evdokimov [21] concluded that more than one growth and dissolution process can occur in the same crystal, revealing precisely the same surface shapes, and may represent overlapping stages of growth and/or dissolution. In our diamonds, the symmetry of their structure was demonstrated by the morphology of the material viewed with SEM-FEG analysis, which found faceted morphology of the CVD Diamond crystals (Figure 2). Particles irradiated by the beam in area 1 are heated and in area 2 are ablated with consequent size reduction, as illustrated in (Figure 3).Water suspensions of laser ablation CVD-DNPs were used to determine the size distribution of the obtained particle through the centrifugation process at 4500 rpm, performed at 0 and 60 min (Table 2).The decreased particle size (Figure 4) was due to the laser ablation and centrifuging time, in which the disagglomeration and stability of CVD-DNPs occurred. This size is very close to that of a single diamond nanocrystallite [22], indicated by the left dislocating curves at 30–60 min ablation time and 0–60 min centrifugation time, where the medium hydrodynamic radius was 54 and 57 nm (Figures 4a-4b). The non-centrifuged CVD-DNPs exhibited the medium size of 72 and 82 nm (Figures 4c-4d), respectively. Furthermore, a wider distribution curve was observed

with laser ablation time, and centrifugation for 60 minute provided the precipitation of larger nanoparticles and average diameter of NDs in suspension. The high stability of aqueous suspension of CVD-DNPs was indicated by the low polydispersity index (PI) (0.2) and a small increase in the mean value of hydrodynamic diameter during the observation period. The high stability was provided by the high charge density on the surface of the NDs, as suggested by the high Zeta-potential (-36.39 and -30.94 mV), respectively (Table 3).

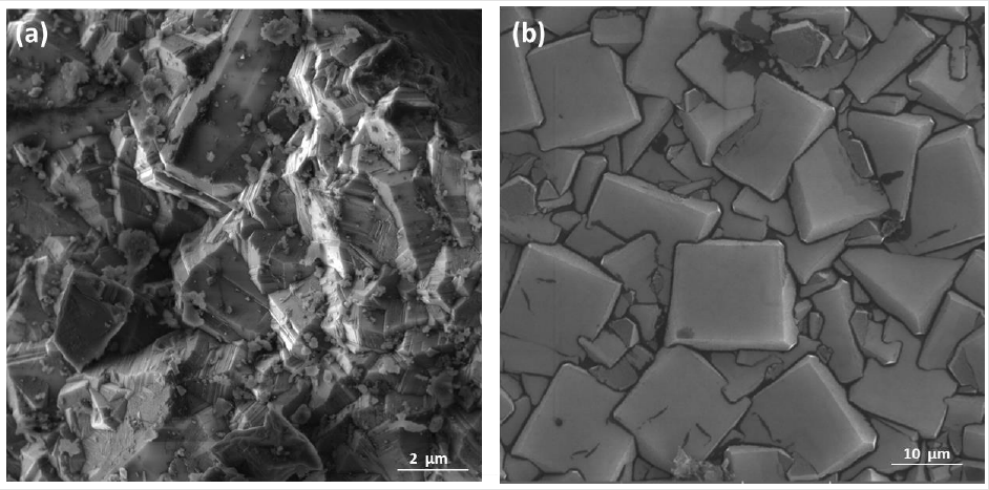


**Figure 2:** Sample surface in CVD Diamond before laser ablation
(a) Magnification of (100 kx);
(b) Magnification of (500 kx).

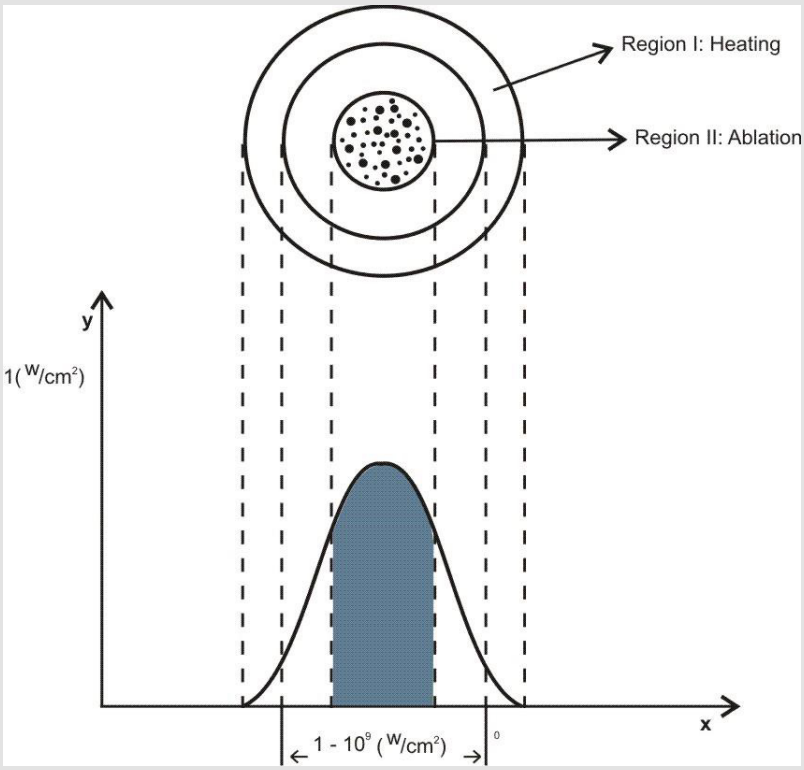


**Figure 3:** Schematic representation of irradiance (w/a) as a function of beam diameter.

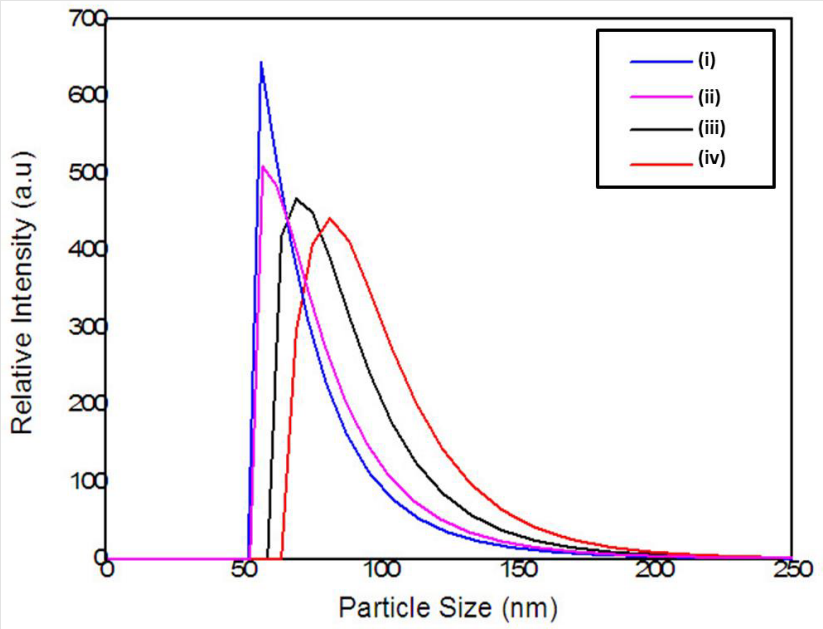


**Figure 4:** Particle size distribution of the
(a) 60 min laser ablation and 60 min centrifugation;
(b) 30 min laser ablation and 60 min centrifugation;
(c) 60 min laser ablation;
(d) 30 min laser ablation without the centrifugation process.

**Table 2:** Particle size distribution data for samples centrifuged for 60 min and different laser ablation times.

| Samples | Laser ablation Time (min) | Centrifugation Time (min) | Average Size(nm) | PDI |
|---|---|---|---|---|
| CVD-DNPs (i) | 30 | 60 | 57±6 | 0.20±0.02 |
| CVD-DNPs (ii) | 60 | 60 | 54±5 | 0.19±0.01 |
| CVD-DNPs (iii) | 30 | 0 | 82 ±7 | 0.31±0.02 |
| CVD-DNPs (iv) | 60 | 0 | 72±6 | 0.26±0.02 |

**Table 3:** Stability of the aqueous suspension Zeta potential CVD-DNPs laser ablation.

| SAMPLES | Hydrodynamic Diameter | PDI | Zeta Potential (mV) |
|---|---|---|---|
| CVD-DNPs (i) | 215.00 ±0.01 | 0.200±0.001 | -36.39 |

According to studies by Koniakhin [23], these z-potential values evidence the produced colloidal stability. Measures were taken in colloidal solutions before and after centrifugation. From the measurements carried out on these solutions, a comparison between the results of the mean hydrodynamic size measurements using SEM and TEM analysis was possible. Purity identification and contaminant ND content were employed to elucidate the characteristics used SEM/TEM [24], XRD [25], Raman Spectroscopy [26], and FTIR [27]. (Figure 5) shows images after laser ablation for 60 min and after centrifugation for 60 min, respectively. The morphological change in the diamonds was due to the process (Figure 5a). The obtained images illustrate the aggregates of CVD formation and the uniform particle size. In addition, the ablated and centrifuged CVD-DNPs are significantly smaller in size. The software image J was employed to analyze the SEM-FEG images, which allowed us to measure the size of CVD-DNPs through a statistical count to find the mean size value of the size distribution for each sample. For each case, using a sample of 100 particles, we obtained the particle size distribution curve, as shown in (Figure 5b). The average particle size of the CVD-NDs before and after centrifugation was 50.62 ± 14.28 nm.Note the morphological difference in (Figure 6) of the average particle size, morphology, and

dispersion of CVD-DNPs after ablation as obtained by transmission electron microscopy (TEM), after centrifugation (Figure 6a). The synthesized CVD-DNPs are agglomerated with rounded shape due to the performed process. (Figure 6b) is the image analyzed with the image J software to estimate size distribution. Thus, analyzing four regions of each sample were, a statistical calculation was done by adding the areas of the CVD-DNPs found in each of the two images taken for each sample. The medium particle size for the samples after centrifugation and laser ablation was 20.50 ± 6.19 nm. In addition, the discrete difference in the ND size evidenced by the Dynamic Light Scattering (DLS) and the Scanning Electron Microscopy (SEM), does not indicate that the results found were.

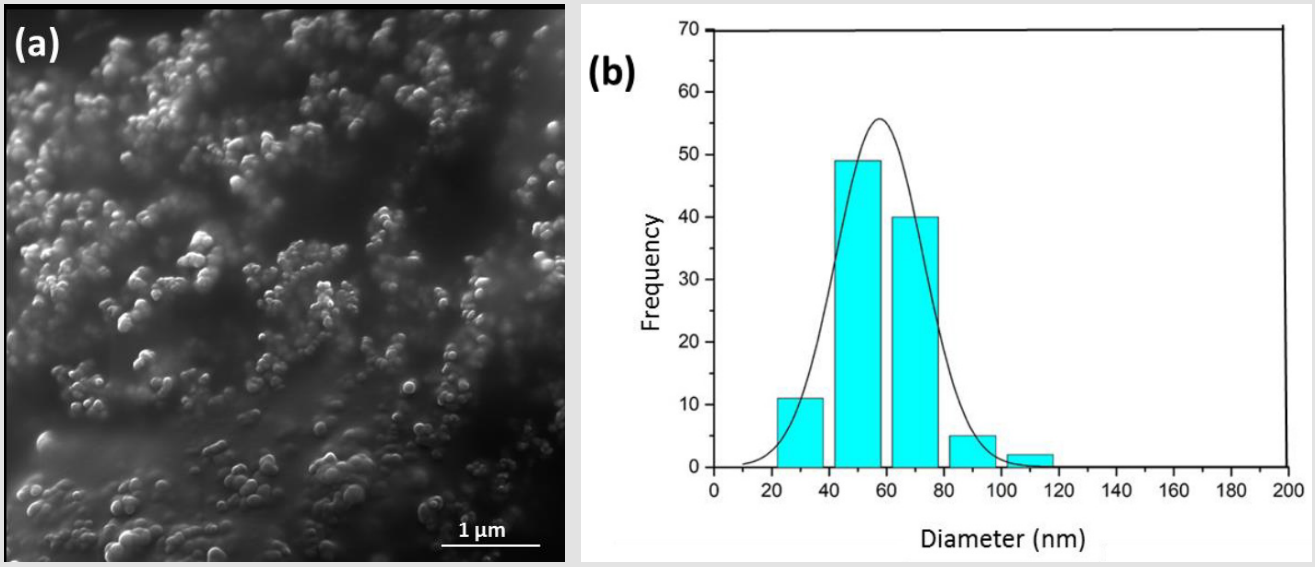


**Figure 5:** SEM images of the particles

(a) Sample after 60 min of laser ablation, 60 min centrifugation and purification (increase of 500kx);

(b) Image distribution of particle sizes, with average size of 50.62 ± 14.28 nm.

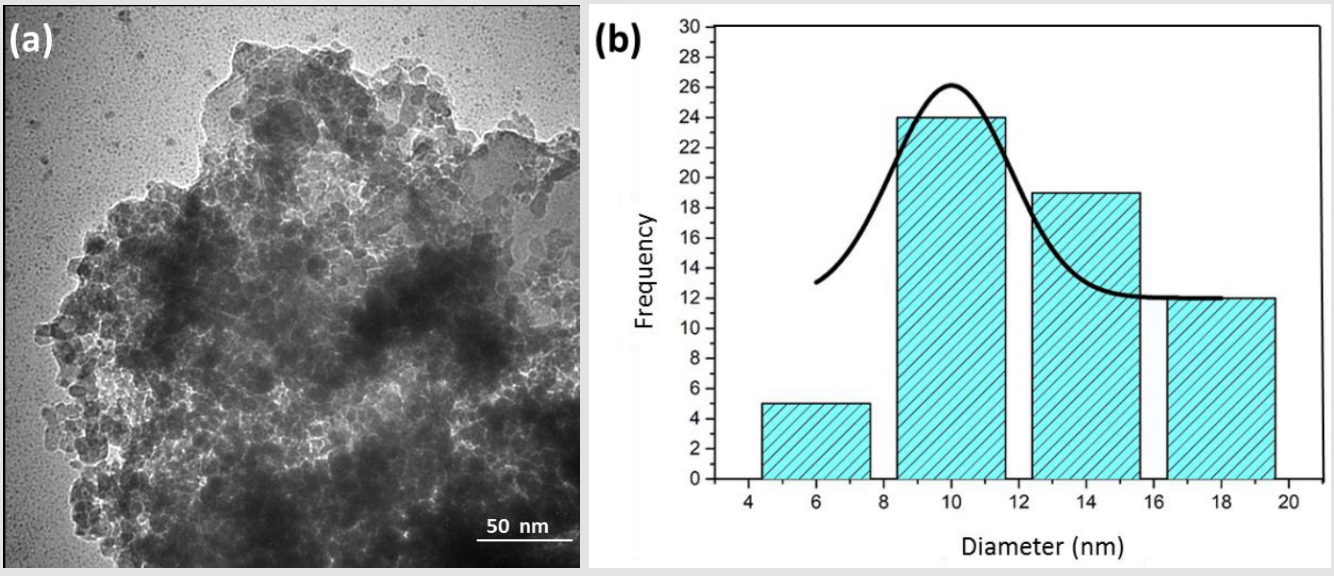


**Figure 6:** TEM images of the particles

(a) Sample after 60 min of laser ablation, with 60 min centrifugation and purification (20 Kx);

(b) Image granulometric distribution, with average size of 20.50 ± 6.19 nm;

Incompatible, because the second method provides only a small portion of the nanoparticles isolated from the medium. With transmission electron microscopy (TEM), the diameters found were between 10 and 20 nm. According to the results, laser ablation time and the centrifugation process produces diamond nanoparticles with nanometric size [28]. The dispersive energy spectroscopy (EDX) was used to analyze the chemical composition of the CVD-DNPs before and after the laser ablation and centrifugation processes. For this analysis, a drop of the colloidal solution was placed under a carbon tape. Due to equipment limitations, we chose a sample region of EDS with larger particles (Figure 7). EDX spectrum with 5 kV energy from laser ablation sample (Figure 8a) shows the mass concentration, where we obtained the same 97.1% carbon and 2.9% oxygen values. Figure 7b presents the mass concentration, where we obtained the same 77.8% carbon and 22.2% oxygen values; and (Figure 7c) exhibits the mass concentration, where we obtained the same 78.3% carbon and 21.7% oxygen values, indicating that carbon is present in these samples. Oxygen concentration is possibly due to high reactivity; in both CVD-DNPs groups, the concentration remained the same. According to Pearce [28], EDX spectra indicated the presence of only C and O; the purified NDs also confirmed the absence of impurities. This result supports those of Yang et al. [29] and confirms that diamond may be produced by ablation under water. Results indicate that, as expected, the final material does not present contamination in the CVD-DNPs from the ablation techniques.

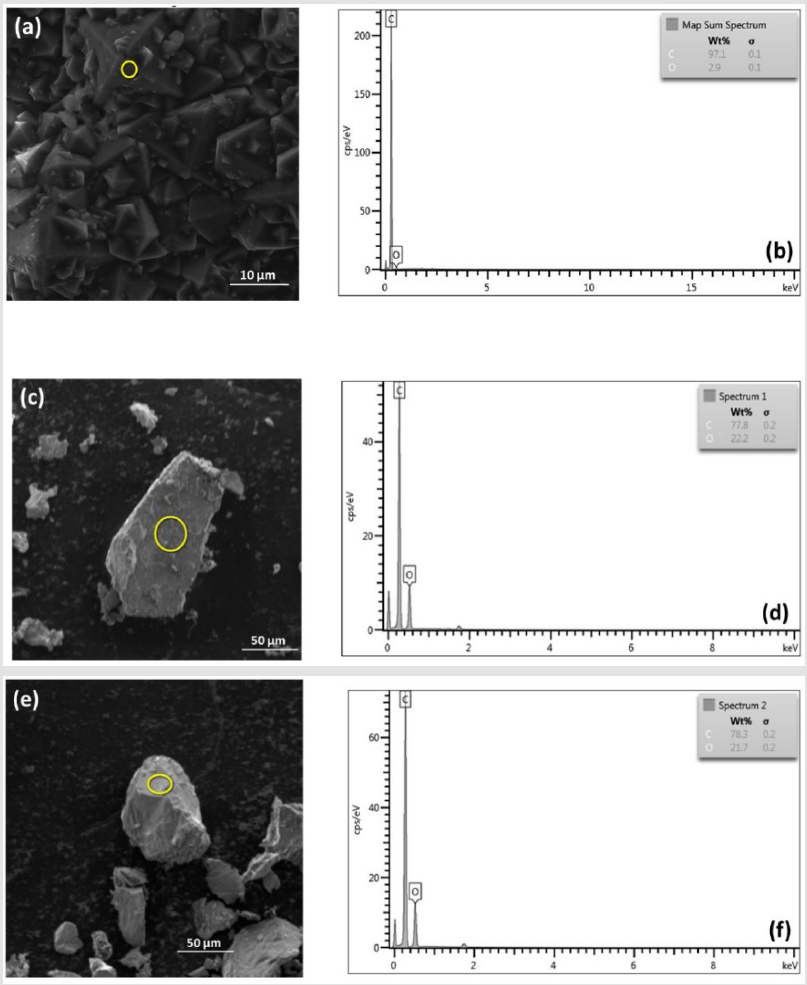


**Figure 7:** EDS graph

(a) CVD diamond;

(b) CVD-NDs;

(c) 30 min laser ablation and 60 min centrifugation, after acid treatment to remove $SiO_2$ from the sample.

(i) CVD-NDs;

(ii) 60 min laser ablation and 60 min centrifugation after acid treatment to remove $SiO_2$ from the sample.

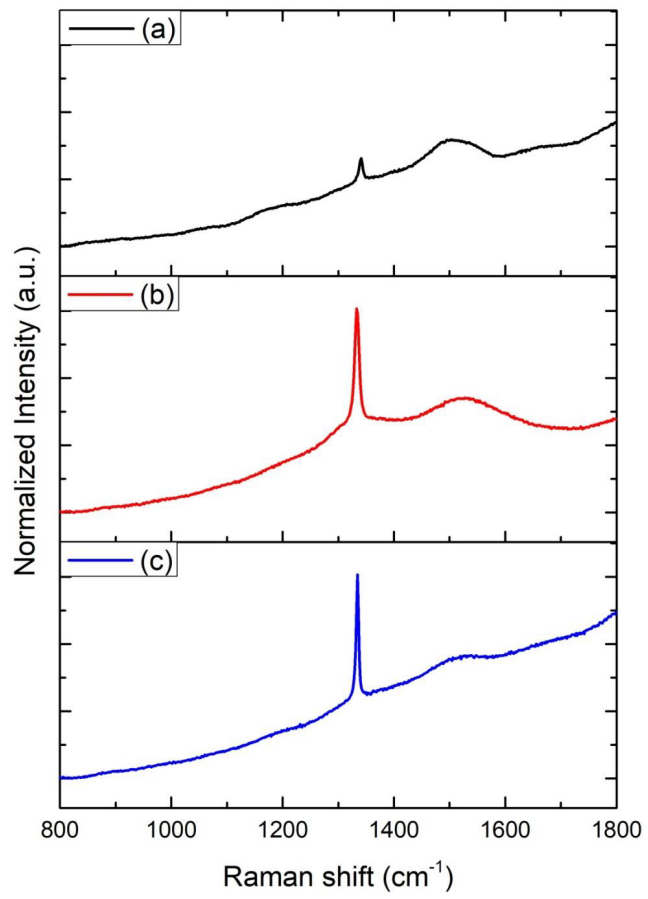


**Figure 8:** XRD graphics:

(a) CVD diamond before laser ablation,

(b) CVD-DNPs

(i) 30 min laser ablation and 60 min centrifugation,

(c) CVD-DNPs

(ii) 60 min laser ablation and 60 min centrifugation,

(d) CVD-DNPs (i) 30 min laser ablation and 60 min centrifugation, after acid treatment to remove $SiO_2$ from the sample, and

(e) CVD-DNPs

60 min laser ablation and 60 min centrifugation after acid treatment to remove $SiO_2$ from the sample;

The Raman spectra of all ND colloids suspensions after the laser ablated CVD-DNPs processing, were measured using a laser Raman spectrometer employing 25% of laser power with wavelength of λ = 532 nm (Figure 9). The material was characterized by Raman spectroscopy, which provides the information of photoluminescence frequency of different carbon structures [30]. The size of the nanodiamonds was also studied using Raman spectroscopy, which also made it possible to determine molecular structures as well as quantify and identify materials and degree of crystalline network disorder. The spectral analysis of the CVD-diamond sample showed the characteristic peak of sp3 hybridization at 1332 cm [31] of a residual stressless diamond [32] (Figure 9a). The band of amorphous carbon, centered at 1550 cm-1, much wider than diamond, was also observed. The peaks, found for all CVD-diamond samples and CVD-DNPs analyzed, confirm the literature data that indicated the Raman shift at 1332.5 ($cm^{-1}$) for carbon in the formation of crystalline diamond, and amorphous carbon at 1550 ($cm^{-1}$) [33]. The evident luminescent background is due to its visibleluminescence spectrum, as well as to the symmetry of the carbon atoms in the form of graphite (sp2 hybridization) on the CVD-diamond crystal and to the continuous emission because of expected crystal defects in CVD-diamond. The laser ablation process reduced the size of the diamond crystals and their luminescence effect in the Raman spectrum, (Figures 9b-9c) respectively, characteristic of structural diamonds.

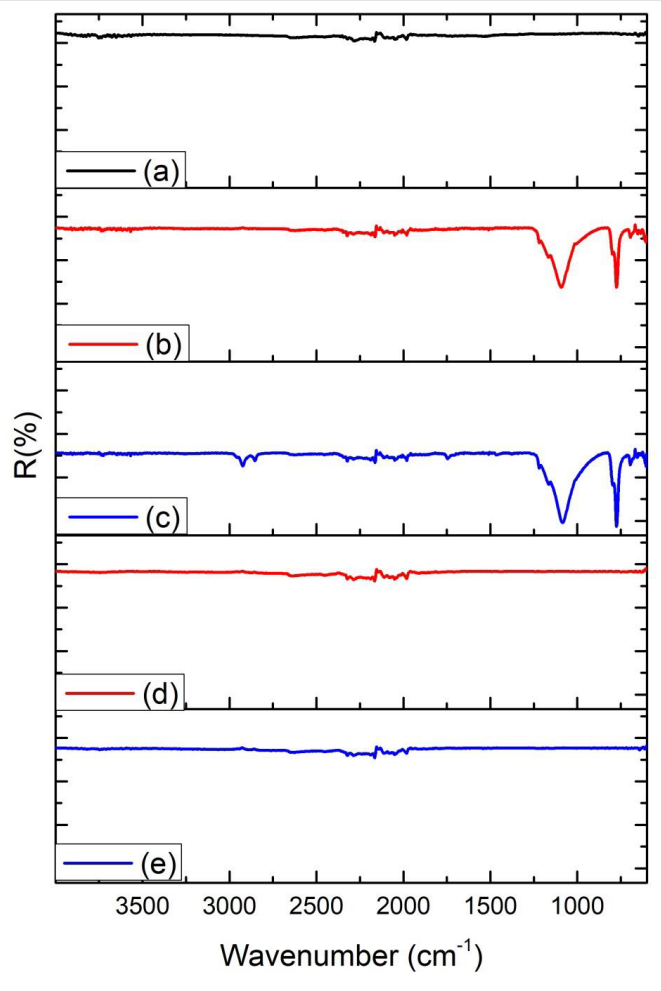


**Figure 9:** Raman spectra intensity (u.a) Vs of
(a) CVD diamond before laser ablation,
(b) CVD-NDs,
(c) 30 min laser ablation and 60 min centrifugation,
(i) CVD-NDs
(ii) 60 min laser ablation and 60 min centrifugation.

Another feature is the principle of incident and dispersed light, where the intensity of the Raman lines is dramatically increased when the scattered light intensity between the incident photons is equal to the permissible electronic interband transition energy [33-36]. Both spectra indicated that the diamond had a high degree of purity, due to the low G-band intensity, which is related to a low graphite inclusion in the diamond, proving the technological efficiency of the process. Therefore, the laser ablation process showed no difference, indicating that the resulting material was not modified. To identify the contamination present in CVD diamond films and CVD-DNPs, a detailed FTIR analysis was performed on each sample as well as those formed the with laser ablation synthesis. This analysis verified whether there were changes in the chemical structure resulting from ablation, since it provides the possibility of functionalization of ND surface to promote biological or materials application. The FT-IR spectra of the CVD-Diamond sample and the CVD-DNPs obtained herein are depicted in (Figure 10). The spectra are presented in a range between 4000 and 400 $cm^{-1}$. Above 4000 $cm^{-1}$, there was no absorption in any of the samples. On the other hand, with the ATR sampling technique used, the absorbances obtained below 400 cm-1 were no longer reliable. Spectrum analysis was performed based on the peak assignment available in the literature [37]. The absence of absorption bands in the FT-IR spectrum of CVD diamond confirmed that this sample did

not have contamination (Figure 10a). The FT-IR spectrum of CVD-DNP laser ablation (Figures 10b-10c) showed very intense bands at 1089 $cm^{-1}$ and 777 $cm^{-1}$, which were attributed to Si-O-Si stretching and bending, suggesting the contamination of the sample with silica due to the agate mortar and pestle, wherein the raw diamond was macerated at the beginning of the process of ND preparation. Despite the contamination with Si-O-Si silica, FT-IR spectrum indicated that NDs obtained herein starting from laser ablation could be eliminated by acid treatment with HF followed by washing with deionizedwater and centrifuged for 300 min. The success of cleaning step could be certified by the absence of Si-O-Si silica absorption band in the FT-IR spectra of cleaned CVD-DNPs obtained herein as depicted in (Figures 10d-10e). Based on the identification and quantification of crystalline phases, the determination of single cell parameters, the orientation of crystallite, and the determination of residual stress [38] and its possible contaminants, we used an X-Ray diffractometer to identify and quantify crystalline phases. The material was characterized by x-ray diffraction before and after laser ablation (Figure 8), using the Highscore software. The observed characteristic diffraction peaks of the diamond, for angles of 2Θ = 43.9°, 75.3°, and 91.5°, were related to the diffraction of the planes (111), (220), and (311), respectively, as shown in (Figure 8a), with Plane (111) being the most intense. This analysis verified that the CVD-DNPs did not present any contamination after laser ablation and purification process of the CVD-DNPs.Using the Scherrer equation [38-40] and the values of the width at half height of the most intense diamond, considering λ=1.54056, it was possible to calculate the crystallite size (Eq.1):

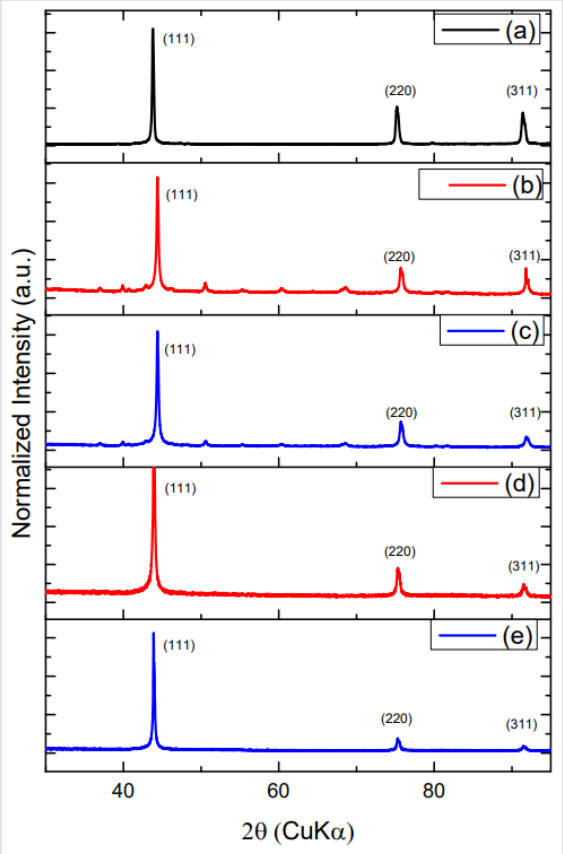


**Figure 10:** FTIR spectra of the:

(a) CVD diamond before laser ablation,

(b) CVD-DNPs

(i) 30 min laser ablation and 60 min centrifugation,

(c) CVD-DNPs

60 min laser ablation and 60 min centrifugation,

(d) CVD-DNPs

(ii) 30 min laser ablation and 60 min centrifugation, after acid treatment to remove $SiO_2$ from the sample, and (e) CVD-DNPs

(iii) 60 min laser ablation and 60 min centrifugation after acid treatment to remove $SiO_2$ from the sample. The FT-IR spectrum was an average of 32 scans at a speed of 2 s per scan in a range of 400–4000 $cm^{-1}$.

(iv) The resolution of the spectrometer was of 4 $cm^{-1}$.

$$D = \frac{k\lambda}{\beta \cos\theta}; (5)$$

Where, D = average size of the crystallite,

*k* = dimensionless form factor,

β = line widening in radians,

θ = Bragg angle, and

λ = X-ray wavelength.

The mean size was determined from the total half-width maximum (FWHM) of the X-ray diffraction peak [41].

The FWHM value includes errors originating from noise and equipment conditions, such as the width of the X-ray diffraction slit. In general, it is difficult to calculate the deconvolutions when the observed signals have high level noise. According to table 4, to obtain the FWHM value of each peak, we used the Voigt line shape approximation by the sum of a Gaussian-type distribution and a Lorentzian width [42]. Sample ablated for 60 minutes had a wider peak, as shown in (Table 4) for all diffraction planes exhibiting a smaller particle size. Likewise, (Figures 8b-8c) shows the orientation of crystallite (111) in the characterization of CVD Diamond after the laser ablation process, and (Figures 8d-8e) indicates that the purification process was efficient for cleaning the CVD-DNPs. In accordance with theoretical studies reported by Telling [43], the Diamond cleavage energy was lower for Plane (111), meaning that there was a priority for the cleavage of the CVD diamond in these crystalline phases. The experimental results presented are coherent with the literature. All observed peaks are in accordance with JCPDS (Joint Committee on Powder Diffraction Standards) no. 00-006-0675 (ND). Considering that one of the main applications of DNPs under investigation in the biomedical field has been drug delivery for cancer therapy [44,45], we evaluated the cytotoxicity of the DNPs prepared herein. The MTT assay was employed for this and offers a quantitative, convenient method to evaluate whether a material affects cell viability.

**Table 4:** Full width at half maximum (FWHM) of the diffraction peaks after laser ablation of CVD-DNPs.

| SAMPLES | Laser ablation Time (min) | FWHM for (111) (º2θ) | FWHM for (220) (º2θ) | FWHM for (311) (º2θ) |
|---|---|---|---|---|
| CVD-DNPs (i) | 30 | 0.376564 | 0.464103 | 0.516482 |
| CVD-DNPs (ii) | 60 | 0.224748 | 0.441423 | 0.309688 |

The extension of MTT reduction by mitochondria of viable cells is proportional to the absorbance of formazan [46]. The cytotoxicity of CVD-DNPs was evaluated against murine melanoma cells B16F10. The MTT assay was performed by incubating cells for 24 h and 48 h with CVD-NDs at 5 different concentrations: CVD-DNPs (0.05 μg/mL), (25 μg/mL), (50 μg/mL), (125 μg/mL), and (250 μg/mL). As depicted in (Figure 11), CVD-DNPs were not cytotoxic to B16 cells after 24 h of incubation at any of the studied concentrations. In this assay, all the values of cell viability were equal or above 70%, considered the standard deviation, which is the limited value accepted to consider a material as non-cytotoxic. This observation is in agreement with the results reported by Schrand et al. [47]. In their work, NDs with 2–10 nm of diameter were not cytotoxic to neuroblastoma cells or macrophages at concentrations in the range of 5–100 μg/mL.Nevertheless, CVD-DNPs showed increased cytotoxicity after 48 h of incubation. At the range of 0.05-125 μg/mL cell viability decreased in function of CVD-DNPs concentration. Interestingly, at the highest concentration of 250 μg/mL, the cell viability was high (76%), indicating non-cytotoxicity at this condition. Increased cytotoxicity after a longer incubation time was not observed by Gismondi, et al. [45], after incubation of B16 and HeLa cells with NDs; however, the authors used smaller DNPs (4-5 nm) and a higher concentration range (5–200 μg/mL). Our results were in line with previous observations of the group and the information found in the literature [48-50]. The cytotoxicity of CVD-DNPs at low concentration is a consequence of the interaction between small nanoparticles with cell membrane, inducing loss of membrane integrity and cell death. On the other hand, when CVD-DNPs are at higher concentration, they are prone to form large aggregates, mainly due to the proteins of the culture medium, which adsorb on ND surfaces. These large structures are not able to insert into cell membrane; thus, the cell viability is not compromised. Therefore, as low cytotoxicity is one of the key features required for a drug delivery platform [47], the NDs prepared in this work have the potential to be used in the cancer therapy, such as melanoma. Notably, the concentration of DNPs suspension has to be carefully controlled. Another alternative is the application of these small DNPs to prepare larger structures wherein several kinds of drugs could be loaded, as already reported [45,47,51].

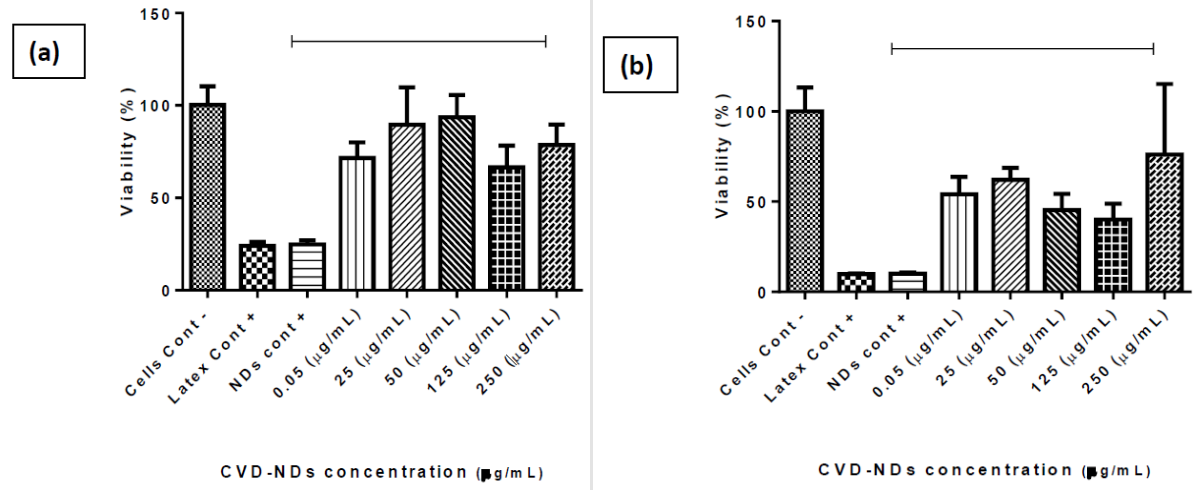


**Figure 11:** B16 F10 murine metastatic melanoma cells viability assessed by MTT assay in cells cultivated for 24 h and 48 h with CVD-NDs produced by laser ablation technique (a–b) at 5 different concentrations. The results are presented as average ± standard error for n = 5 (One Way ANOVA test and Tukey multiple comparisons). Incubation of CVD-NDs without cells followed by the incubation with MTT and measurement of absorbance was performed to evaluate possible interfering signals from CVD-NDs (CVD-NDs control).

## Conclusion

The synthetic diamond-CVD, which has the same physical and chemical properties as natural diamonds, was useful to synthesize DNPs by Laser ablation (ytterbium doped fiber laser). It was possible to obtain DNPs with average hydrodynamic diameter of 54 nm and a particle size distribution between -2–10 nm. These CVD-DNPs properties favor the adsorption or complexation with other compounds, and the cell internalization due to their small size. The cost of diamonds is become less, encouraging the use of this important class of materials for a variety of applications, especially biological ones. The cell viability assay evidenced low cytotoxic of CVD-DNPs. The incubation of murine metastatic melanoma B16-F10 cells with CVD-DNPs for 24 h and 48 h resulted in cell viability of 70–80% at 250 µg/mL. The low cytotoxicity against tumor cells indicated the potential use of CVD-DNPs as drug delivery platforms for antitumoral therapy. The conjugation of photosensitizers (PS) CVD-DNPs and cytolocation will be investigated in future stages of this research.

## Declarations

### Ethics Approval and Consent to Participate

Not applicable.

### Consent for Publication

Not applicable.

### Availability of Data and Material

All data generated or analyzed during this study are included in this published article.

### Competing Interests

The authors declare that there is no conflict of interest.

### Funding

The Fundação de Amparo à Pesquisa do Estado de São Paulo (FAPESP) (grant numbers 2012/15857-1; 2017/01697-6; 2017/01697-6; and 2012/15857-1), the National Council for Scientific and Technological Development (CNPq) (grant number 380402/2019-0), and the Coordination for the Improvement of Higher Education Personnel (CAPES).

### Authors' Contributions

All authors were involved in writing the manuscript. All authors contributed to the experimental design. All authors read and approved the final manuscript.

### Acknowledgement

The authors want to acknowledge support from Institute for Advanced Sea Studies (IEAMar/UNESP) and Brazilian National Council for Scientific and Technological (CNPq). Ministry of Science, Technology and Innovation (MCTI) and the PRO marking company, for the use of ytterbium doped pulsed fiber laser.

## References

1. May PW (1995) CVD diamond: a new technology for the future?. 19(3): 101-106.
2. Nemanich RJ, Carlisle JA, Hirata A, Haenen K (2014) CVD diamond - Research Applications, and challenges MRS Bulletin 39(6): 490-494.
3. Engineering B, Cha C, Shin SR, Annabi N and Dokmeci MR (2013) Carbon-Based Nanomaterials. Multifunctional Materials for Biomedical Engineering. 7(4): 2891-2897.

4. Ansari SA, Satar R, Jafri MA, Rasool M, Ahmad W, et al. (2016) Role of Nanodiamonds in Drug Delivery and Stem Cell Therapy.Iranian Journal of Biotechnology 14(3): 130-141.
5. Holt KB (2007) Diamond at the nanoscale Applications of diamond nanoparticles from cellular biomarkers to quantum computing Philosophical Transactions of the Royal Society. A Mathematical Physical and Engineering Sciences 365(1861): 2845-2861.
6. Mona J, Tu JS, Kang TY, Tsai CY, Perevedentseva E, et al. (2012) Surface modification of nanodiamond Photoluminescence and Raman Studies. Diamond and Related Materials 24: 134138.
7. Xing Y, Dai L (2009) Nanodiamonds for nanomedicine. Nanomedicine 4(2): 207-218.
8. Verma A, Uzun O, Hu Y, Hu Y, Han HS, et al. (2008) Surface-structure-regulated cell-membrane penetration by monolayer-protected nanoparticles. Nature Materials 7: 588-595.
9. Setyawati MI, Mochalin VN Leong DT (2016) Tuning endothelial permeability with functionalized nanodiamonds. ACS Nano 10 1170-1181.
10. El-say K M 2011 El-Say, 2011.pdf 01 29-39
11. Li J, Zhu Y, Li W, Zhang X, Peng Y, et al. (2010) Nanodiamonds as intracellular transporters of chemotherapeutic drug. Biomaterials 31(32): 8410-8418.
12. Krueger A (2008) Diamond nanoparticles. Jewels for chemistry and physics Advanced Materials 20(12): 2445-2249.
13. Turcheniuk K, Mochalin VN (2017) Biomedical applications of nanodiamond (Review). Nanotechnology 28(25): 252001.
14. Zeng H, Du XW, Singh SC, Kulinich SA, Yang S, et al. (2012) Nanomaterials via laser ablation irradiation in liquid A review. Advanced FunctionalMaterials 22(7): 1333-1353.
15. Amendola V, Meneghetti M (2013) What controls the composition and the structure of nanomaterials generated by laser ablation in liquid solution. Physical Chemistry Chemical Physics 15(9): 3027-3046.
16. Tan D, Lin G, Liu Y, Teng Y, Zhuang Y, et al. (2011) Synthesis of nanocrystalline cubic zirconia using femtosecond laser ablation. Journal of Nanoparticle Research 13(3): 1183-1190.
17. Tan D, Xu B, Chen P, Dai Y, Zhou S, et al. (2012) One-pot synthesis of luminescent hydrophilic silicon nanocrystals. RSC Advances 22: 8254-8257.
18. Tan D, Zhou S, Xu B, Chen P, Shimotsuma Y, et al. (2013) Simple synthesis of ultra-small nanodiamonds with tunable size and photoluminescence. Carbon 62: 374-381.
19. Kvick A (2016) X-Ray Diffraction Materials Science Applications Encyclopedia of Spectroscopy and Spectrometry, pp. 648-655
20. Fidler IJ (1975) Biological Behavior of Malignant Melanoma Cells Correlated to Their Survival *in Vivo*. Cancer Research 35(1): 218-224.
21. Evdokimov MD, Ladygina MY, Nesterov AR (2001) Morphology of diamonds as a possible indicator of their genesis. Neues Jahrbuch fur Mineralogie Abhandlungen 176(2): 153-177.
22. Dideikin T, Aleksenskii AE, Baidakova MV, Brunkov PN, Brzhezinskaya M, et al. (2017) Rehybridization of carbon on facets of detonation diamond nanocrystals and forming hydrosols of individual particles. Carbon 122: 737-45.
23. Koniakhin SV, Besedina NA, Kirilenko DA, Shvidchenko AV, Eidelman ED (2018) Ultracentrifugation for ultrafine nanodiamond fractionation. Superlattices and Microstructures 113: 204-212.
24. Shames AI, Panich AM, Kempiński W, Alexenskii AE, Baidakova MV, et al (2002) Defects and impurities in nanodiamonds EPR NMR and TEM study. Journal of Physics and Chemistry of Solids 63(11): 1993-2001.
25. Costa GCC, Shenderova O, Mochalin V, Gogotsi Y, Navrotsky A (2014) Thermochemistry of nanodiamond terminated by oxygen. containing functional groups Carbon 80(1): 544-550.
26. Mermoux M, Crisci A, Petit T, Girard HA, Arnault JC, et al. (2014) Surface modifications of detonation nanodiamonds probed by multiwavelength raman spectroscopy. Journal of Physical Chemistry C 118: 23415-23425.
27. Petit T, Puskar L (2018) FTIR spectroscopy of nanodiamonds Methods and interpretation. Diamond and Related Materials 89: 52-66.
28. Pearce SRJ, Henley SJ, Claeyssens F, May PW, Hallam KR, et al. (2004) Production of nanocrystalline diamond by laser ablation at the solid. y liquid interface 13: 661-665.
29. Nistor LC, Epurescu G (1998) Preparation of nano-crystalline diamonds using pulsed laser induced reactive quenching Preparation of nano-crystalline. diamonds using pulsed laser induced reactive quenching.
30. Ferrari AC, Robertson J (2004) Raman spectroscopy of amorphous, nanostructured, diamond-like carbon, and nanodiamond Philosophical Transactions of the Royal Society A Mathematical. Physical and Engineering Science 362: 2477-512.
31. Ager JW, Drory MD (1993) Quantitative measurement of residual biaxial stress by Raman spectroscopy in diamond grown on a Ti alloy by chemical vapor. deposition Physical Review B 48: 2601-2617.
32. Michler J, Mermoux M, Von Kaenel Y, Haouni A, Lucazeau G, et al. (1999) Residual stress in diamond films: Origins and modelling. Thin Solid Films 357: 189-201.
33. Knight DS, White WB (1989) Characterization of diamond films by Raman spectroscopy. 4(2): 385-393.
34. Moskovits M (2005) Surface-enhanced Raman spectroscopy A brief retrospective. Journal of Raman Spectroscopy 36(6): 485-496.
35. Kneipp K, Kneipp H, Itzkan I, Dasari RR, Feld MS (2002) Ultrasensitive Chemical Analysis by Raman Spectroscopy. Chemical Reviews 99: 2957-2976.
36. Determination PS (1939) No Title 56: 978-982.
37. Dischler B, Wild C, Koidl P (1993) Hydrogen in polycrystalline diamond 185.
38. Kvick Å (2017) X-Ray Diffraction, Materials Science Applications Encyclopedia of Spectroscopy and Spectrometry, pp. 648-655
39. Bestimmung A, Klasse M, Klasse M, Dokument D, Copyright D, et al. (1918) Nutzungsbedingungen.
40. Wilson AJC (1978) Palouse_StableIsotopes_SedFingerprinting_2003, pp. 102-113.
41. Birks L S, Friedman H (1946) Particle size determination from x-ray line broadening. Journal of Applied Physics 17: 687-92
42. Wertheim GK, Butler MA, West KW, Buchanan DNE (1974) Determination of the Gaussian and Lorentzian content of experimental line shapes. Review of Scientific Instruments 45: 1369-1371.
43. Telling RH, Pickard CJ, Payne MC Field JE (2000) Theoretical Strength and Cleavage of Diamond. 84(22):5160.
44. Jimenez CM, Knezevic NZ, Rubio YG, Szunerits S, Boukherroub R, et al. (2016) Nanodiamond-PMO for two-photon PDT and drug delivery. Journal of Materials Chemistry B 4 35: 5803-5808.

45. Gismondi A, Reina G, Orlanducci S, Mizzoni F, Gay S, et al. (2015) Nanodiamonds coupled with plant bioactive metabolites: A nanotech approach for cancer therapy. Biomaterial 38: 22-35.

46. Wan H, Williams R, Doherty P, Williams DF (1994) A study of the reproducibility of the MTT test. Journal of Materials Science Materials in Medicine 5: 154-159.

47. Schrand AM, Huang H, Carlson C, Schlager JJ, Osawa E, et al. (2007) Are diamond nanoparticles cytotoxic. Journal of Physical Chemistry B 11: 2-7.

48. Eldawud R, Reitzig M, Opitz J, Rojansakul Y, Jiang W (2016) Combinatorial approaches to evaluate nanodiamond uptake and induced cellular fate. Nanotechnology 27(8): 85107.

49. Chatterjee A, Perevedentseva E, Jani M, Cheng CY, Ye YS, et al. (2014) Antibacterial effect of ultrafine nanodiamond against gram-negative bacteria Escherichia coli. Journal of Biomedical Optics 20(5): 051014.

50. Woodhams B, Ansel-Bollepalli L, Surmacki J, Knowles H, Maggini L, et al. (2018) Graphitic and oxidised high pressure high temperature (HPHT) nanodiamonds induce differential biological responses in breast cancer cell lines. Nanoscale 10: 12169-12179.

51. Wu MS, Sun DS, Lin YC, Cheng CL, Hung SC, et al. (2015) Nanodiamonds protect skin from ultraviolet B-induced damage in mice. Journal of Nanobiotechnology 13(1): 1-12.

**ISSN: 2574-1241**

DOI: 10.26717/BJSTR.2022.41.006604

**Cristiane Da Costa Wachesk.** Biomed J Sci & Tech Res



**Submission Link**: https://biomedres.us/submit-manuscript.php